J Fluoresc (2011) 21:203–211
DOI 10.1007/s10895-010-0706-1

ORIGINAL PAPER

Photoluminescence of Rare Earth Phosphors $Na_{0.5}Gd_{0.5}WO_4$: RE^{3+} and $Na_{0.5}Gd_{0.5}(Mo_{0.75}W_{0.25})O_4$: RE^{3+} (RE = Eu, Sm, Dy)

Bing Yan · Lixia Lin · Jianhua Wu · Fang Lei

Received: 20 April 2010 / Accepted: 19 July 2010 / Published online: 30 July 2010

Abstract Two series of phosphors, $Na_{0.5}Gd_{0.5}WO_4$: RE^{3+} and $Na_{0.5}Gd_{0.5}(Mo_{0.75}W_{0.25})O_4$: RE^{3+} (RE=Eu, Sm, Dy) have been synthesized by hydrothermal process to obtain the high purity, which have been characterized by X-ray powder diffraction (XRD), scanning electron microscope (SEM). The results suggest that $Na_{0.5}Gd_{0.5}(Mo_{0.75}W_{0.25})O_4$: RE^{3+} phosphors are more easily to crystallize than $Na_{0.5}Gd_{0.5}WO_4$: RE^{3+} ones. Both of them present the characteristic luminescence of Eu^{3+}, Sm^{3+} and Dy^{3+}. Especially the photoluminescent properties of $Na_{0.5}Gd_{0.5}WO_4$: x% Eu^{3+} (Sm^{3+}) can be obtained to show white luminescence as the suitable doping concentration of Eu^{3+} or Sm^{3+}.

Keywords Luminescence · Hydrothermal synthesis · Microstructure · Rare earth ions

Introduction

Recently there has been a growing concern about phosphor-converted light-emitting diodes (LEDs) and tricolor phosphors, which are widely considered as the next generation of solid state illumination materials [1–4]. In these devices, the tricolor phosphors are pumped by UV-InGaN chips or blue GaN chips and generate white light. Nowadays one of the challenges for the new generation of lighting based upon GaN comes from the development of novel families of phosphors that are optimized for excitations at longer wavelengths in the near UV (350–400 nm). The current phosphor materials of choice for solid state lighting based upon near UV GaN-LEDs are Y_2O_2S: Eu^{3+} for red, ZnS: (Cu^+, Al^{3+}) for green, and $BaMgAl_{10}O_{17}$: Eu^{2+} for blue. However, the efficiency of the Y_2O_2S: Eu^{3+} red phosphor is much less than that of the green and blue phosphors except that its lifetime is severely limited by the dose of UV irradiation [5, 6]. Therefore, the primary interest of the present works is just to search for novel red phosphors for near UV InGaN chip-based white light-emitting diodes.

Tungstate and molybdate compounds are important functional inorganic materials, which can be applied in the fields of phosphor, scintillator, photocatalyst and gas sensor, *etc* [7–10]. Among double tungstate and molybdates $ARE(MO_4)_2$ (A=Li^+, Na^+ and some K^+; RE=trivalent rare earth ions, M=Mo^{6+}, W^{6+}) which shares scheelite-like structure, have been widely studied because of their laser applications [11–14]. The scheelite-like structure of $CaMO_4$ (M=Mo, W) is tetragonal crystal system with space group symmetry $I4_1/a$, and Ca^{2+} can be substituted by a combination of a monovalent and a trivalent cation, leading to the formation of $AR(MO_4)_2$ (M=Li, Na, R=Ln, Y, Bi, M=Mo, W) compounds with a statistical distribution of M^+ and RE^{3+}. Among the photoluminescent properties of double molybdates doped europium have been investigated by many researchers [5, 15].

As we known, rare earth ions doped tungstates are developed for the laser or luminescent materials. Lately, complex tungstate-molybdates $ARE(MO_4)_2$ (A=alkali metal ions, M=Mo, W) have become the hot spot for the atoms Mo and W, which have similar ionic radius, to substitute each other. In this paper, two series of phosphors, $Na_{0.5}Gd_{0.5}WO_4$: RE^{3+} and $Na_{0.5}Gd_{0.5}(Mo_{0.75}W_{0.25})O_4$: RE^{3+} (RE=Eu, Sm, Dy) have been synthesized by a facile hydrothermal process. Considering the blue emission of host, we doped three kinds of photoactive rare earth ions

B. Yan (✉) · L. Lin · J. Wu · F. Lei
Department of Chemistry, Tongji University,
Shanghai 200092, People's Republic of China
e-mail: byan@tongji.edu.cn

and obtain the white luminescence by modifying the doping concentration of them.

Experimental

Synthesis

RE_2O_3 (99.99 %) (RE=Eu, Sm, Dy) and $Na_2MO_4{\cdot}2H_2O$ (AR) (M=Mo, W) are used without any further purification. $RENO_3)_3{\bullet}6H_2O$ are prepared by dissolving the corresponding oxides in diluted nitric acid, and at last the crystal of these hydrate are obtained by heating carefully.

Stoichiometric amounts of $Gd(NO_3)_3{\bullet}6H_2O$, $RE(NO_3)_3{\bullet}6H_2O$ (RE=Eu, Sm, Dy, whose doping concentrations are 0. 2, 0.5, 1, 2, 5 mol %; totally 1.0 mmol) are mixed uniformly using 5 mL distilled water. $Na_2MO_4{\bullet}2H_2O$ (M=Mo, W) is also dissolved into 5 mL distilled water and then added to the above rare earth nitrate solution. After 30 min, the mixed solution is sealed in a Teflon-lined stainless steel autoclave with a volume of 20 mL. The solution is heated at 220°C for 8 h ($Na_{0.5}Gd_{0.5}WO_4$: RE^{3+}), 2 h ($Na_{0.5}Gd_{0.5}(Mo_{0.75}W_{0.25})O_4$: RE^{3+}) and cooled to room temperature. The resulting powders are washed several times with distilled water by centrifugation, and finally suspended in ethanol then dried at 60°C for 24 h. The scheme of for the synthesis can be shown as below:

$$0.5Na_2Mo_yW_{1-y}O_4 \cdot 2H_2O\,(y = 0,\ 0.75) + (1-x)Gd(NO_3)_3 \cdot 6H_2O + xRE(NO_3)_3 \cdot 6H_2O \rightarrow$$
$$Na_{0.5}Gd_{0.5}Mo_yW_{1-y}O_4 : xRE^{3+} + 3NaNO_3 + xH_2O(RE = Eu,\ Sm,\ Dy;\ x = 0.2,\ 0.5,\ 1,\ 2,\ 5\,mol\%)$$

Characterization

X-ray diffraction (XRD) is carried out on a Bruck D8-Advance diffractometer with CuKα radiation (0.15405 nm). The accelerating voltage and emission current are 40 kV and 40 mA, respectively. SEM images are obtained using a Philips XL-30 to observe the morphology and microstructure of samples; and TEM images are obtained using a JEOL 1230 transmission electron microscope operating at 200 kV. Samples for TEM are prepared by depositing a drop of a colloidal ethanol solution of the powder sample onto a carbon coated copper grid. The excess liquid was wicked away by filter paper, and the grid is dried in air. The excitation and emission spectra are taken on an RF-5301 spectrophotometer which is equipped with a 150 W xenon lamp as the excitation source. All the emission and excitation spectra are corrected and the intensities are determined with integrated area. Luminescent lifetimes for hybrid materials are obtained with an Edinburgh Instruments FLS 920 phosphorimeter using a 450 W xenon lamp as excitation source (pulse width, 3 μs).

Results and Discussion

Figure 1 presents the selected XRD patterns of the different systems. Figure 1(a) is for the XRD pattern of product after 2 h' hydrothermal treatment and can be seen that the crystal phase of $Na_{0.5}Gd_{0.5}WO_4$: $5\%Eu^{3+}$ have not formed completely, but the (112) plane at $2\theta=28$ °has appeared. After 8 h' hydrothermal reaction, the product is well crystallized to form the crystal phase of $Na_{0.5}Gd_{0.5}WO_4$: $5\%Eu^{3+}$ (see Fig. 1(b)), which indicates that prolonging hydrothermal reaction time is favorable for the improvement of crystallization degree of product. It is very consistent with the JCPDS file 25-0829 [$Na_{0.5}Gd_{0.5}WO_4$], showing that the sample has a single phase with the scheelite structure of space group centrosymmetric I41/a [16] and tetragonal crystal system, whose unit cell parameters are a=b=5.243 Å, c=11.368 Å and possesses the low symmetry lack of inversion center. Different from $Na_{0.5}Gd_{0.5}WO_4$: $5\%Eu^{3+}$, well-crystallization of $Na_{0.5}Gd_{0.5}MoO_4$: $5\%Eu^{3+}$ can be obtained after 2 h' hydrothermal reaction, which is shown in Fig. 1(c) and suggests the different metal ion still has apparent influence on the reaction behavior in spite of

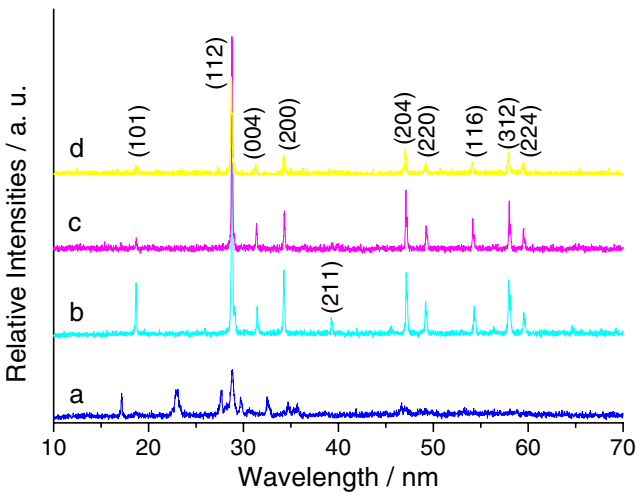

Fig. 1 X-rays diffraction patterns of (**a**) $Na_{0.5}Gd_{0.5}WO_4$: $5\%Eu^{3+}$ (2 hr), (**b**) $Na_{0.5}Gd_{0.5}WO_4$: (8 hr), (**c**) $Na_{0.5}Gd_{0.5}MoO_4$: $5\%Eu^{3+}$ (2 hr), (**d**) $Na_{0.5}Gd_{0.5}(Mo_{0.75}W_{0.25})O_4$: $5\%Eu^{3+}$ (2 hr)

similar physical property of W^{6+} and Mo^{6+}. The XRD pattern (Fig. 1d) $Na_{0.5}Gd_{0.5}(Mo_{0.75}W_{0.25})O_4$5%$Eu^{3+}$ is the same as that of $Na_{0.5}Gd_{0.5}MoO_4$: 5%Eu^{3+}. This reveals that the substitution of Mo by W has not change the structure of $Na_{0.5}Gd_{0.5}MoO_4$: 5%Eu^{3+} and the solid solution of $(Mo_{0.75}W_{0.25})O_4^{2-}$ forms. All these products can not be checked the hybrid phase in their XRD patterns. The approximate particle size of the product is estimated from (112) peak according to the Debye-Scherrer's equation:

$$D = 0.89\lambda/(\beta \times \cos\theta) \quad (1)$$

where D is the average grain size, λ represents Cu Kα wavelength 0.1542 nm and β is the half-width of the peak with Bragg angle θ. The calculated results show that the average crystallite sizes of $Na_{0.5}Gd_{0.5}WO_4$: 5%Eu^{3+}, $Na_{0.5}Gd_{0.5}MoO_4$: 5%Eu^{3+} and $Na_{0.5}Gd_{0.5}(Mo_{0.75}W_{0.25})O_4$: 5%$Eu^{3+}$ are around 100 nm, 50 nm and 80 nm, respectively.

The FT-IR spectra of the as-synthesized samples $Na_{0.5}Gd_{0.5}WO_4$: 5%Eu^{3+} and $Na_{0.5}Gd_{0.5}(Mo_{0.75}W_{0.25})O_4$: 5%$Eu^{3+}$ phosphors by hydrothermal technology at 220°C are shown in Fig. 2. The IR spectrum of $Na_{0.5}Gd_{0.5}WO_4$: 5%Eu^{3+} phosphor has approximately same vibration modes as that of $Na_{0.5}Gd_{0.5}$ $(Mo_{0.75}W_{0.25})O_4$: 5%Eu^{3+}. The bands at 3363 cm^{-1} and 1649 cm^{-1} are assigned to O-H stretching vibration and H-O-H bending vibration, respectively [17, 18]. The two bands are the characteristic vibrations of water molecules from air physically absorbed on the sample surface, which is completely different from coordinated water in compounds. The 1380 cm^{-1} band is attributed to the N-O vibration modes probable from the remaining starting reactants NO_3^-. A strong absorption band around 803 cm^{-1} is related to O-W-O stretches of WO_4 tetrahedron or O-Mo-O stretches of MoO_4 tetrahedron because the AWO_4 type sheelite oxides have S_4 site symmetry for the WO_4^{2-} groups and show the main absorption bands in the region of 400–1000 cm^{-1}, centered around 911, 833 and 405 cm^{-1} corresponding to the ν_1, ν_3 and ν_2 modes of the WO_4^{2-} groups, respectively [20]. From the same reason, the 451 cm^{-1} band is attributed to ν_2 stretching vibration of W-O or Mo-O.

Figure 3 (a, b) shows the selected SEM images of $Na_{0.5}Gd_{0.5}WO_4$: 5%Eu^{3+} and $Na_{0.5}Gd_{0.5}(Mo_{0.75}W_{0.25})O_4$: 5%$Eu^{3+}$, respectively. Both of the products consist of sub-micrometer Spindle-like flakes, indicating that the similar growth mechanism in the hydrothermal process for the similar property of W and Mo element. Besides, the spindle-like flake particle size of $Na_{0.5}Gd_{0.5}WO_4$: 5 %Eu^{3+} is bigger than that of $Na_{0.5}Gd_{0.5}(Mo_{0.75}W_{0.25})O_4$: 5%$Eu^{3+}$. This may be ascribed the fact that the hydrothermal reaction time of the former (8 h) is more than that of the latter (only 2 h).

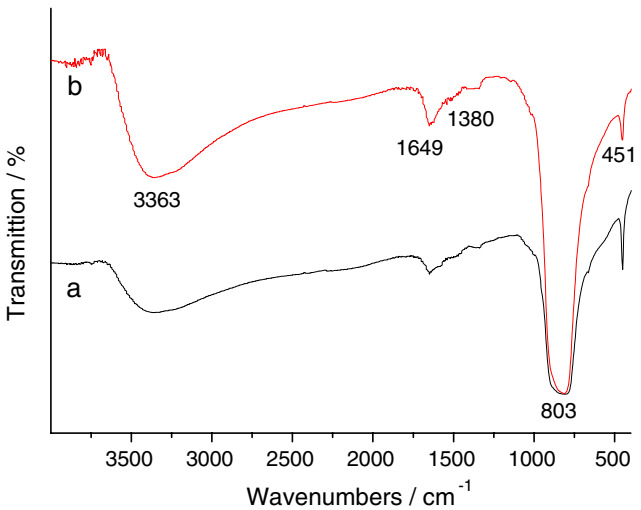

Fig. 2 FT-IR spectra of (**a**) $Na_{0.5}Gd_{0.5}WO_4$: 5%Eu^{3+} and (**b**) $Na_{0.5}Gd_{0.5}(Mo_{0.75}W_{0.25})O_4$: 5%$Eu^{3+}$

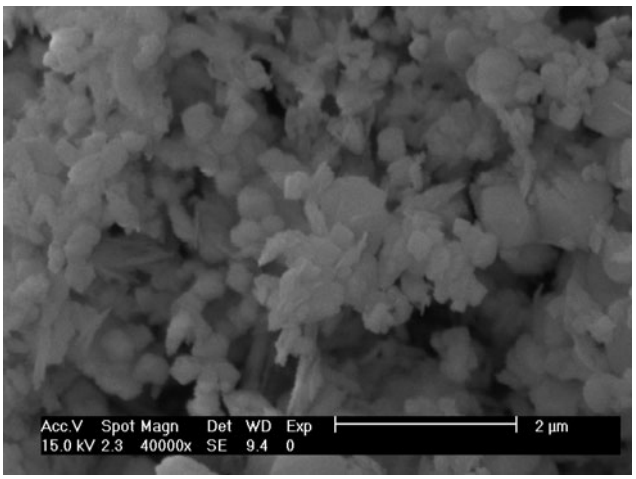

a Selected SEM image of (a) $Na_{0.5}Gd_{0.5}WO_4$

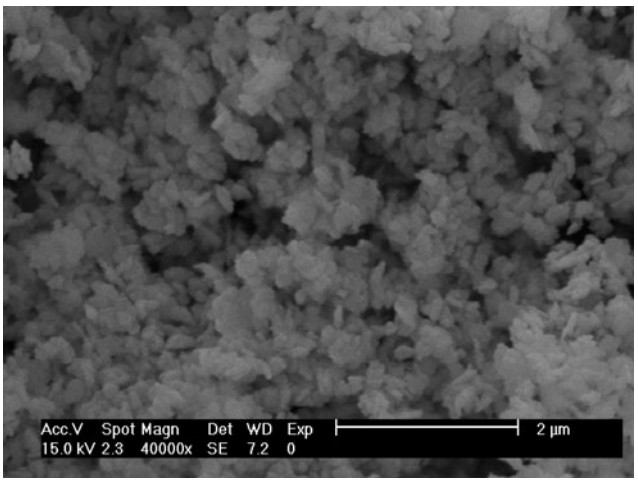

b Selected SEM image of $Na_{0.5}Gd_{0.5}(Mo_{0.75}W_{0.25})O_4$

Fig. 3 Selected SEM image of (**a**) $Na_{0.5}Gd_{0.5}WO_4$: 5%Eu^{3+} and (**b**) $Na_{0.5}Gd_{0.5}(Mo_{0.75}W_{0.25})O_4$: 5%$Eu^{3+}$

The UV-vis diffuse reflectance absorption spectra of $Na_{0.5}Gd_{0.5}WO_4$: 5%Eu^{3+} and $Na_{0.5}Gd_{0.5}(Mo_{0.75}W_{0.25})O_4$: 5 % Eu^{3+} are shown in Fig. 4. They both have broad absorption band ranged from 200 to 400 nm and the spectrum of $Na_{0.5}Gd_{0.5}(Mo_{0.75}W_{0.25})O_4$: 5% Eu^{3+} (half band width 80 nm) is steeper than that of $Na_{0.5}Gd_{0.5}WO_4$: 5 mol % Eu^{3+} (half band width 100 nm). The similar feature can be found in the Fig. 4 (b) for Sm^{3+} doped system and Fig. 4 (c) for Dy^{3+} doped system. All these figures indicate that MoO_4^{2-} has broader absorption band than WO_4^{2-} in the UV-light region.

Figures 5 and 6 present the selected excitation and emission spectra of $Na_{0.5}Gd_{0.5}WO_4$: Eu^{3+} and $Na_{0.5}Gd_{0.5}(Mo_{0.75}W_{0.25})O_4$: Eu^{3+}, respectively. The excitation spectra that collected at the emission wavelength of 615 nm show a broad band in the short ultraviolet region within the range between 200 and 350 nm (see Figs. 5(a), 6(b)). The short ultraviolet excitation spectrum with a maximum centered 280 nm can be ascribed to the O→Mo(W) charge transfer state (CTS) from host $Mo_yW_{1-y}O_4^{2-}$ group. This overall efficient excitation transitions are not restricted by parity selection rule and becomes predominant (broad and intense). Compared to the value of 270 nm reported in references [19], the charge transfer band observably shifts toward long wavelength. It is well known that the energy of charge transfer transition from the coordinated atoms (L) to central metal ions (M) is sensitive to the covalency of M–L bond, which is determined by such factors such as the electronegativity difference between M and L, the coordination number of M, the M–L bond length, etc. Here in our phosphors systems, the center metal ion (M) is W and Mo, which is not different from the reference. The sharp lines in 350–450 nm range are ascribed to intra-configurational 4*f*–4*f* transitions of Eu^{3+} in the host lattice ($^7F_0 \rightarrow {}^5D_4$, $^7F_0 \rightarrow {}^5L_7$, $^7F_0 \rightarrow {}^5L_6$, $^7F_0 \rightarrow {}^5D_2$), and the strongest excitation peaks are at 393 nm ($^7F_0 \rightarrow {}^5L_6$). The strong CTS from host MoO_4^{2-} group is favorable for the effective energy transfer and luminescence of Eu^{3+}. While the apparent excitation bands at around 324 nm are related to the $^8S \rightarrow {}^6P$ transition of Gd^{3+}, which is possible to be detected due to the $Gd^{3+} \rightarrow Eu^{3+}$ energy transfer [20, 21]. For the other higher energy level f-f transitions of Gd^{3+} at 275 and 313 nm corresponded to $^8S \rightarrow {}^6I$ and $^8S \rightarrow {}^6P$ have not be checked for they maybe overlapped with the broad LMCT band. In addition, comparing the excitation spectra of these two systems, it can be seen that the excitation from host LMCT of $Na_{0.5}Gd_{0.5}(Mo_{0.75}W_{0.25})O_4$: x%Eu^{3+} is strong while the excitation from the f-f transition is weak, but it is not too apparent for $Na_{0.5}Gd_{0.5}(Mo_{0.75}W_{0.25})O_4$: x%$Eu^{3+}$ system. This suggests that the distinction of host composition still have influence on the excited state absorption of the whole luminescent system.

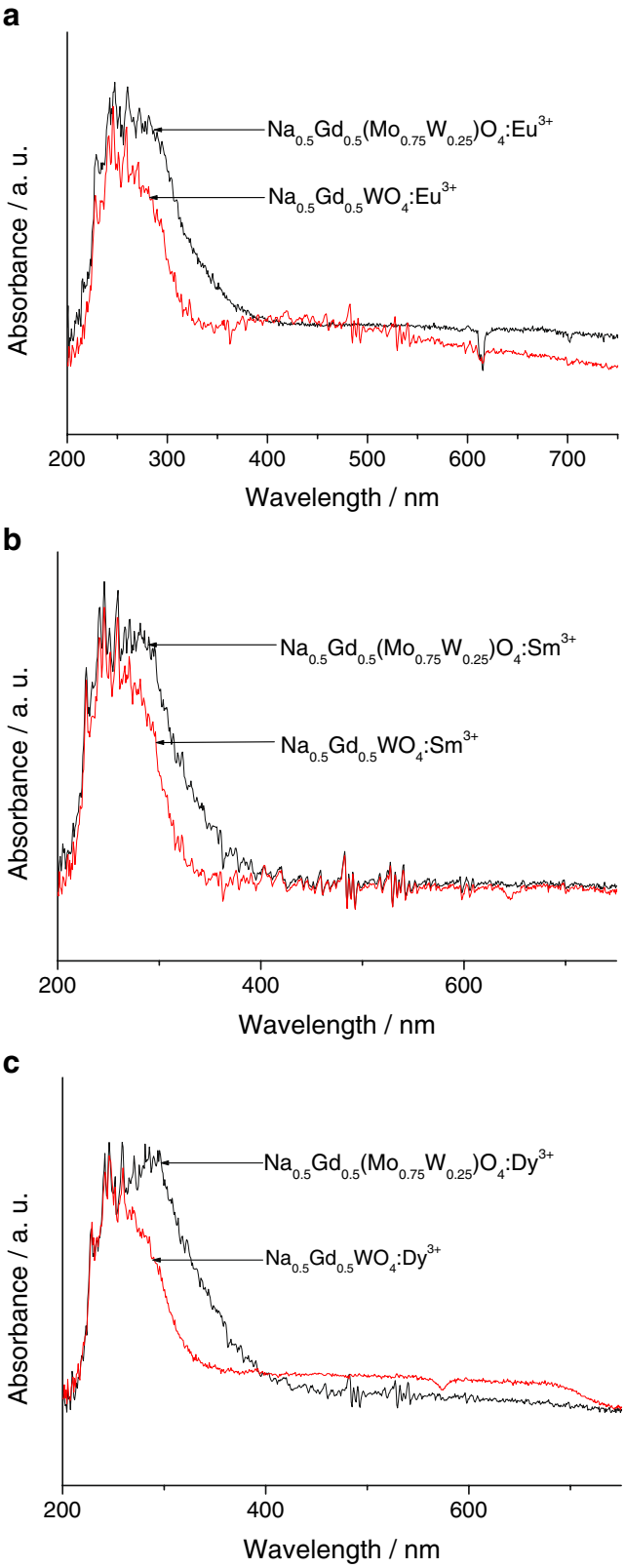

Fig. 4 Selected UV-visible diffusion reflenctance absorption specta of: 5%Eu^{3+} (**a**), 5%Sm^{3+} (**b**), 5%Dy^{3+} (**c**) doped $Na_{0.5}Gd_{0.5}WO_4$ and $Na_{0.5}Gd_{0.5}(Mo_{0.75}W_{0.25})O_4$ phosphors

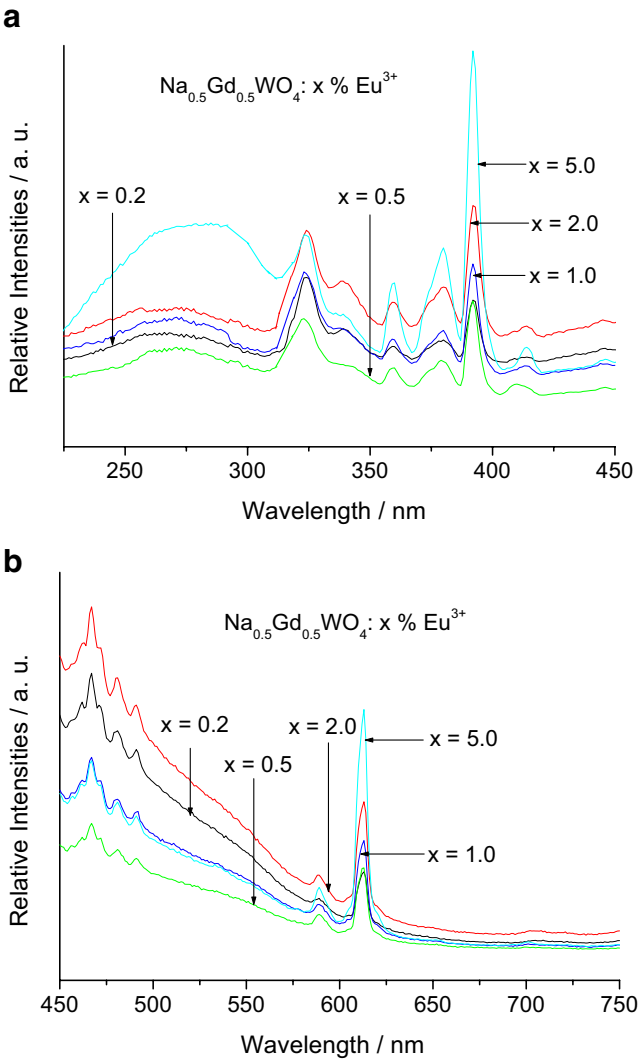

Fig. 5 Excitation (**a**) and emission (**b**) spectra of $Na_{0.5}Gd_{0.5}WO_4$: x%Eu^{3+} phosphors

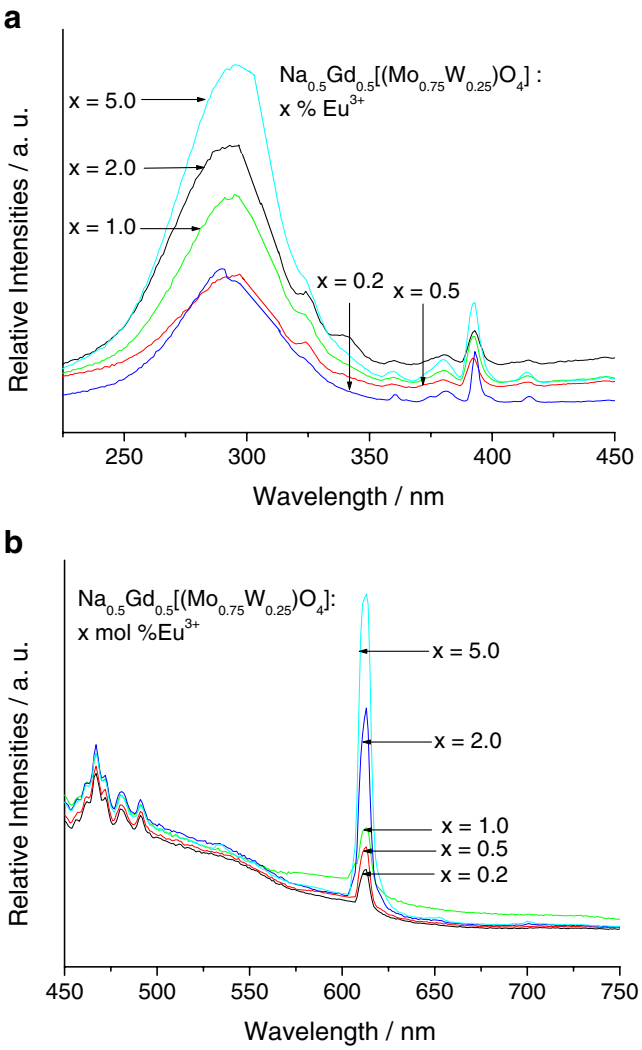

Fig. 6 Excitation (**a**) and emission (**b**) spectra of $Na_{0.5}Gd_{0.5}(Mo_{0.75}W_{0.25})O_4$: x%$Eu^{3+}$ phosphors

The emission spectra (Figs. 5(b), 6(b)) of $Na_{0.5}Gd_{0.5}WO_4$: Eu^{3+} and $Na_{0.5}Gd_{0.5}(Mo_{0.75}W_{0.25})O_4$: Eu^{3+} under the excitation wavelength of 393 nm both show the characteristic emission of Eu^{3+}. Among for $Na_{0.5}Gd_{0.5}WO_4$: Eu^{3+}, the $^5D_0 \rightarrow {}^7F_1$ (592 nm), $^5D_0 \rightarrow {}^7F_2$ (616 nm) lines can be observed. To analyze the transitions observed in the luminescence spectrum, the crystal field splitting of the energy levels has also to be taken into account. The most intense transitions is observed in the luminescence spectrum originate from the $^5D_0$ level, which is not split by the crystal field ($J=0$). In accordance with Judd-Ofelt theory, transitions to even J-numbers have much higher intensity than those to corresponding neighboring odd J-number. In $Na_{0.5}Gd_{0.5}WO_4$: Eu^{3+} phosphors, Eu^{3+} ion replaces Gd^{3+} lattice site. And the luminescent results also reveal that he dominated red peak located at about 614 nm, which comes from the hypersensitive transition $^5D_0 \rightarrow {}^7F_2$ with $\Delta J=2$. This is a parity forbidden f-f intraconfigurational transition. When the Eu^{3+} is located at a low-symmetry local site lack of inversion center, the emission at transition is dominated in the emission spectra [19, 22, 23]. To the point of practical application, strong red emission of $Na_{0.5}Gd_{0.5}WO_4$: Eu^{3+} phosphors under 393 nm light excitation suggest that the compounds are suitable to be excited by a near UV InGaN chip on one hand. For $Na_{0.5}Gd_{0.5}(Mo_{0.75}W_{0.25})O_4$: x%Eu^{3+}, the emission for $^5D_0 \rightarrow {}^7F_1$ transition can not be checked, indicating that Eu^{3+} is located in the environment deviating from the inversion center. Under excitation of ultraviolet lamp, it can be found the white luminescence of $Na_{0.5}Gd_{0.5}(Mo_{0.75}W_{0.25})O_4$: x%$Eu^{3+}$ at the doping concentration of Eu^{3+} is x=0.2, 0.5, 1.0 mol%. Besides, there exist broad band with some splits ranged from 450 to 550 nm, peaking at 467 nm in the blue region, which assigned to the O→W ligand-to-metal charge-transfer states for tungstates belong to the self-activated luminescence

Table 1 Selected luminescent lifetimes and quantum efficiencies of $Na_{0.5}Gd_{0.5}WO_4$: x%Eu^{3+} phosphos

$Na_{0.5}Gd_{0.5}WO_4$: x%Eu^{3+}	x=0.2	x=0.5	x=1.0	x=2.0	x=5.0
$\upsilon_{01}(cm^{-1})$	16978	16978	16978	16978	16978
$\upsilon_{02}(cm^{-1})$	16313	16313	16313	16313	16313
I_{02} / I_{01}	1.41	1.97	2.10	1.84	3.36
A_{0j} (s^{-1})	50, 73	50, 103	50, 110	50, 96	50, 175
A_{rad} (s^{-1})	123	153	160	146	225
τ (μs)	474	504	732	894	1128
A_{exp} (s^{-1})	2109	1984	1366	1118	886
η(%)	5.83	7.71	11.71	13.06	25.40

and the characteristic emission of WO_4^{2-} is still remained. Comparing the two series of Eu^{3+} activated phosphors, it can be found that the 467 nm's emission intensities $Na_{0.5}Gd_{0.5}(Mo_{0.75}W_{0.25})O_4$: x%$Eu^{3+}$ are weaker than those of $Na_{0.5}Gd_{0.5}WO_4$: x%Eu^{3+}, which can be due to the replacement of WO_4^{2-} by MoO_4^{2-} (molybdate can not produce the self-activated luminescence). Finally, it can also be seen that the luminescence intensity become stronger with the increase of the doping concentration of Eu^{3+}, suggesting that no concentration quenching effect can be found in the range of our experiment (0.1–5 mol % Eu^{3+}).

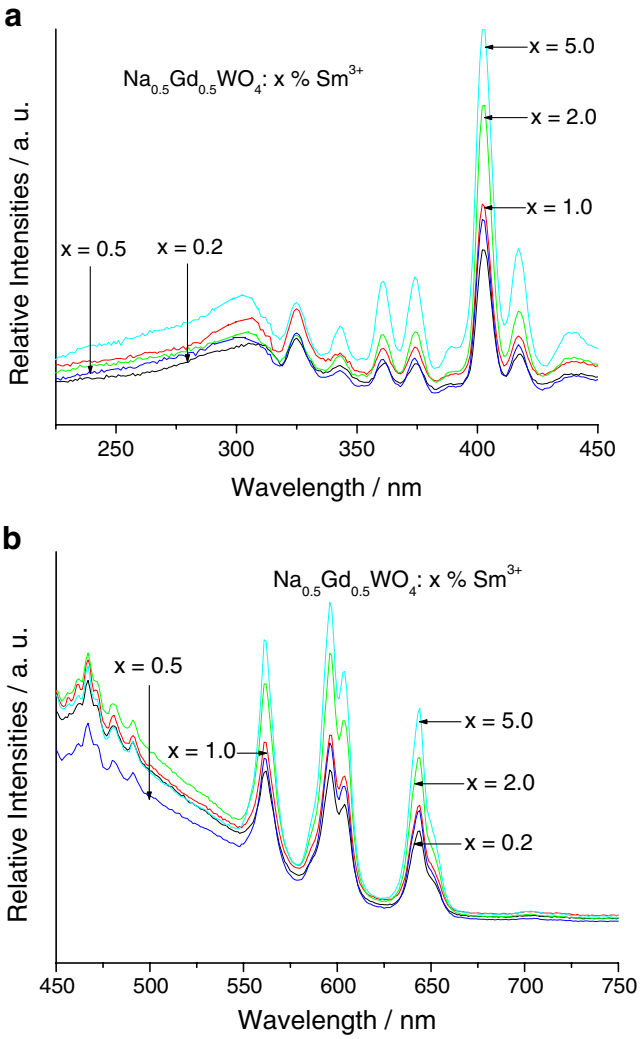

Fig. 7 Excitation (**a**) and emission (**b**) spectra of $Na_{0.5}Gd_{0.5}WO_4$: x%Sm^{3+} phosphors

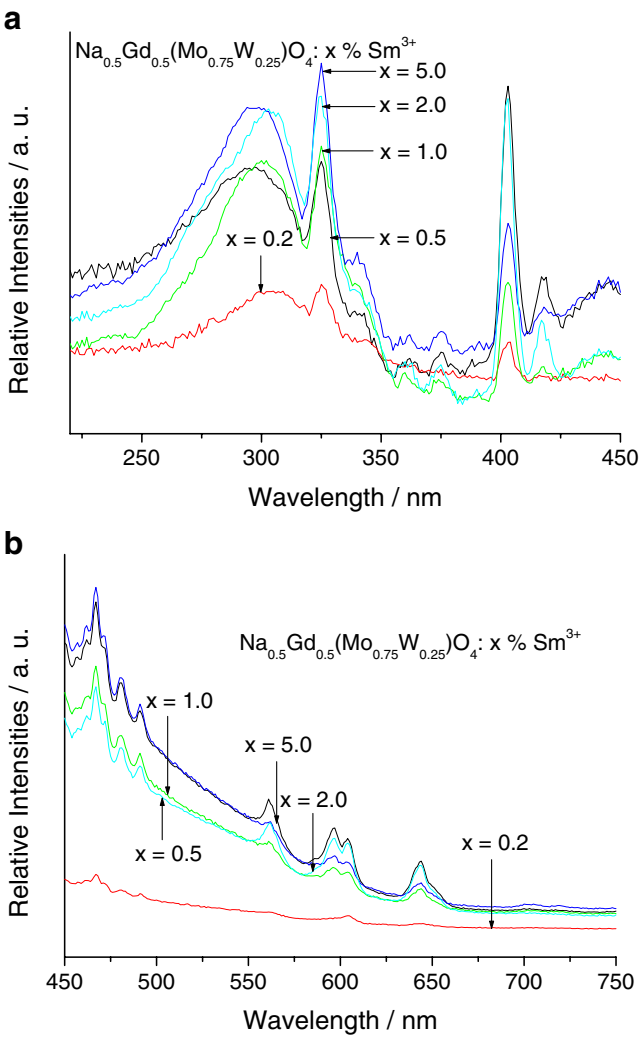

Fig. 8 Excitation (**a**) and emission (**b**) spectra of $Na_{0.5}Gd_{0.5}(Mo_{0.75}W_{0.25})O_4$: x%$Sm^{3+}$ phosphors

The selected typical decay curves of the Eu activated $Na_{0.5}Gd_{0.5}WO_4$ are measured and they can be described as a single exponential ($Ln(S(t)/S_0)=-k_1t=-t/\tau$), indicating that all Eu^{3+} ions occupy the same average coordination environment. The luminescence lifetimes of $Na_{0.5}Gd_{0.5}WO_4$: x%Eu^{3+} are increased with the increasing of the doping concentration of Eu3+, which take agreement with the luminescent intensity. Furtherly, we selectively determined the emission quantum efficiencies of the $^5D_0$ excited state of europium ion for $Na_{0.5}Gd_{0.5}WO_4$: x%Eu^{3+} on the basis of the emission spectra and lifetimes of the $^5D_0$ emitting level. In general, radiative lifetime for a rare earth activated system is well discussed in the framework of JO model. Considering the unique properties of Eu^{3+} ion, and in particular the MD character of the $^5D_0$–$^7F_1$ transition, it is very easy to obtain the radiative lifetimes from the ratio of the integrated intensities as mentioned by the authors. The discussion about lifetime, which needs the following six equations in the papers can reduced to one equation as reported in the ref. [24–28]. The quantum efficiency of the luminescence step, η expresses how well the radiative processes (characterized by rate constant A_r) compete with non-radiative processes (overall rate constant A_{nr}) [24–28].

$$\eta = A_r/(A_r + A_{nr}) \quad (2)$$

The quantum efficiency can be calculated from radiative transition rate constant and experimental luminescence lifetime. The branching ratio for the $^5D_0 \rightarrow {}^7F_{5,\,6}$ transitions can be neglected as they both are not detected experimentally, whose influence can be ignored in the depopulation of the $^5D_0$ excited state [24–28]. Since $^5D_0 \rightarrow {}^7F_1$ belongs to the isolated magnetic dipole transition, it is practically independent of the chemical environments around the Eu^{3+} ion, and thus can be considered as an internal reference for the whole spectrum, the experimental coefficients of spontaneous emission, can be calculated

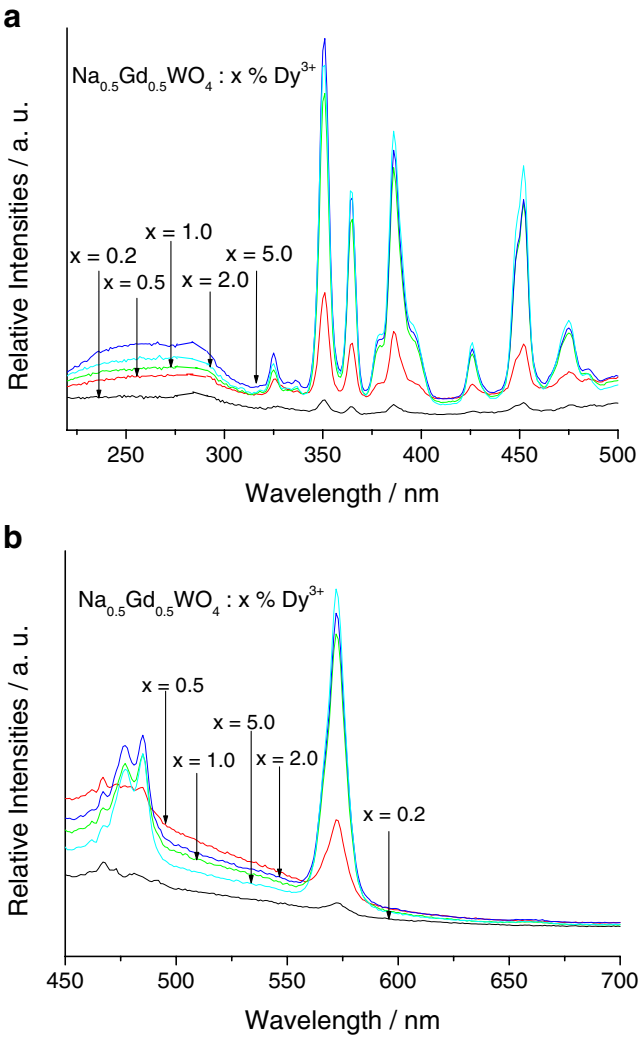

Fig. 9 Excitation (**a**) and emission (**b**) spectra of $Na_{0.5}Gd_{0.5}WO_4$: x% Dy^{3+} phosphors

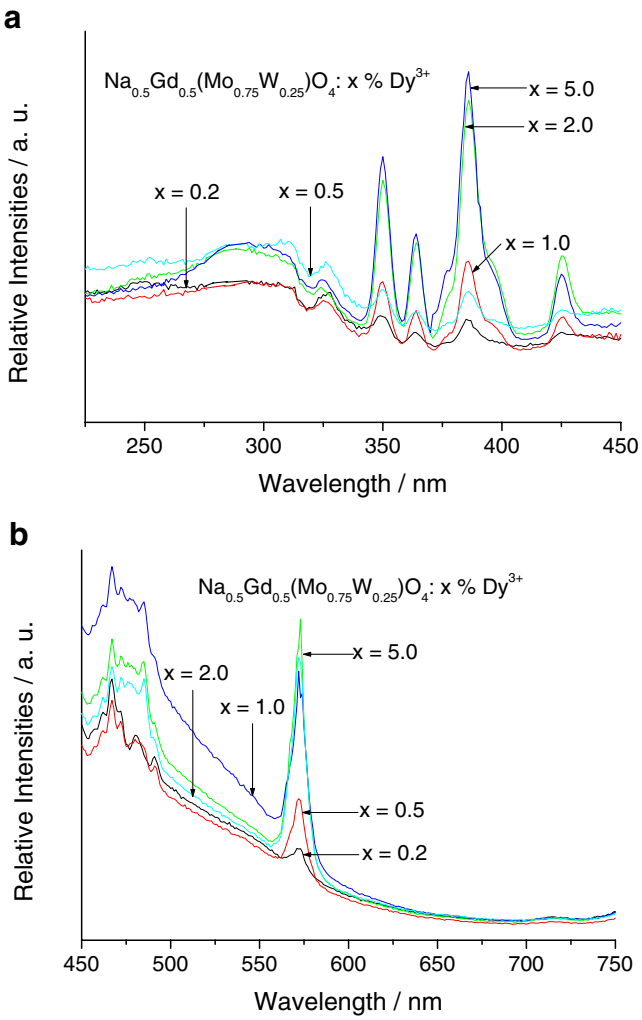

Fig. 10 Excitation (**a**) and emission (**b**) spectra of $Na_{0.5}Gd_{0.5}(Mo_{0.75}W_{0.25})O_4$: x%$Dy^{3+}$ phosphors

with the Einstein's coefficient of spontaneous emission between the $^5D_0$ and $^7F_1$ energy levels (which can be determined to be a constant 50 s^{-1} approximately) [24–28] from the emission spectra. On the basis of the above discussion, the quantum efficiencies of $Na_{0.5}Gd_{0.5}WO_4$: x%Eu^{3+} can be estimated and the detailed data are shown in Table 1, which shows the similar order to the luminescent intensity and lifetime. Here we have to point out the physical mechanism for the non-radiative energy relaxation in the system. The thermal deactivation process is the main factor determining the non-radiative energy loss.

Figures 7 and 8 present the excitation and emission spectra of $Na_{0.5}Gd_{0.5}WO_4$: 5%Sm^{3+} and $Na_{0.5}Gd_{0.5}(Mo_{0.75}W_{0.25})O_4$: 5%$Sm^{3+}$, respectively. The excitation spectra that collected at the emission wavelength of 600 nm show the similar feature to those of Eu^{3+} activated systems. A broad band in the short ultraviolet region within the range between 200 and 350 nm, which can be attributed to the O→Mo(W) charge transfer state (CTS) from host $Mo_yW_{1-y}O_4^{2-}$ group and are not restricted by parity selection rule and becomes predominant (broad and intense). Besides, there exist sharp excitation bands at around 325 nm which overlapped with the CTS bands, corresponding to the $^8S→^6P$ transition of Gd^{3+} possible to be detected due to the $Gd^{3+}→Sm^{3+}$ energy transfer [20, 21]. Obviously, there are some narrow emission lines in the long wavelength region of 350–450 nm, which are originated from the intra-configurational 4*f*-4*f* transitions of Sm^{3+} from the $^6H_{5/2}$ ground state to the $^4G_{9/2}$ (440 nm), $^6P_{5/2}$ (418 nm), $^6G_{11/2}$ (404 nm), $^6P_{7/2}$ (375 nm), $^4D_{5/2}$ (361 nm) states (and the strongest excitation peaks are at 404 nm ($^6H_{5/2}→^6G_{11/2}$) [29, 30]. Comparing the excitation spectra of these two system, it can be seen that the excitation intensity ratio of f-f transition to CTS of $Na_{0.5}Gd_{0.5}WO_4$: 5%Sm^{3+} is more than that of $Na_{0.5}Gd_{0.5}(Mo_{0.75}W_{0.25})O_4$: 5%Sm^{3+} system, revealing that the different host compositions affect the excited state absorption of the whole luminescent system. There exist the apparent difference between the emission spectra of $Na_{0.5}Gd_{0.5}WO_4$: 5%Sm^{3+} and $Na_{0.5}Gd_{0.5}(Mo_{0.75}W_{0.25})O_4$: 5%$Sm^{3+}$. For $Na_{0.5}Gd_{0.5}WO_4$: 5%Sm^{3+}, we can obtain the predominant characteristic emission of Sm^{3+}, which are located at 563 nm ($^4G_{5/2}→^6H_{5/2}$), 601 nm ($^4G_{5/2}→^6H_{7/2}$), and 645 nm ($^4G_{5/2}→^6H_{9/2}$), respectively. The emission for $^4G_{5/2}→^6H_{11/2}$ transition is too weak to be checked. Among the orange transition ($^4G_{5/2}→^6H_{7/2}$) exhibits the strongest emission. While $Na_{0.5}Gd_{0.5}(Mo_{0.75}W_{0.25})O_4$: 5% Sm^{3+} presents much weak emission bands for these $^4G_{5/2}→^6H_J$ transition of Sm^{3+}. Accordingly, the self-activated luminescence of WO_4^{2-} host of $Na_{0.5}Gd_{0.5}WO_4$ are not so apparent as that of $Na_{0.5}Gd_{0.5}(Mo_{0.75}W_{0.25})O_4$, suggesting the $Na_{0.5}Gd_{0.5}WO_4$ is benefit for the luminescence and energy transfer for Sm^{3+}.

Figures 9 and 10 wear the selected excitation and emission spectra of $Na_{0.5}Gd_{0.5}WO_4$: 5%Dy^{3+} and $Na_{0.5}Gd_{0.5}(Mo_{0.75}W_{0.25})O_4$: 5%$Dy^{3+}$, respectively. From the excitation spectra that collected at the emission wavelength of 574 nm, a number of transitions can be observed in the excitation spectra all obviously originating in the $^6H_{15/2}$ ground state: $^4F_{9/2}$ (475 nm), $^4I_{15/2}$ (452 nm), $^4G_{11/2}$ (426 nm), $^4I_{13/2}+^4K_{17/2}+^4I_{17/2}$ (387 nm), $(^4P, ^6P)_{3/2}$ (366 nm) [29, 30]. Among the $^6H_{15/2}→^4I_{13/2}+^4K_{17/2}+^4I_{17/2}$ transitions possess the strongest emission at 387 nm. In the short wavelength of ultraviolet region, two apparent excitation bands can be observed. One is the broad bands at the range of 200 to 320 nm derived from the O→Mo (W) charge transfer state (CTS) from host $Mo_yW_{1-y}O_4^{2-}$ group. The other is the narrow bands with 326 nm, corresponding to the $^8S→^6P$ transition of Gd^{3+} possible to be detected due to the $Gd^{3+}→Dy^{3+}$ energy transfer [20, 21]. Two characteristic emission bands of Dy^{3+} appear, 485 nm and 573 nm. Both the emissions correspond to the characteristic transitions of Dy^{3+} ion, blue transition ($^4F_{9/2}→^6H_{15/2}$) and yellow one ($^4F_{9/2}→^6H_{13/2}$), respectively. Among the yellow emission ($^4F_{9/2}→^6H_{13/2}$) belongs to the strongest and the blue emission is overlapped with the host emission.

Conclusion

In summary, hydrothermal technology is to synthesize $Na_{0.5}Gd_{0.5}WO_4$: x%RE^{3+} and $Na_{0.5}Gd_{0.5}(Mo_{0.75}W_{0.25})O_4$: x%$RE^{3+}$ (RE=Eu^{3+}, Sm^{3+}, Dy^{3+}). X-ray powder diffraction (XRD), scanning electron microscope (SEM) and transmission electron microscope (TEM) indicate that there exist some flake-like crystals with the scheelite structure and the mean particle size is about sub-micrometer order. The luminescent behavior for three rare earth ions activated phosphors have been studied and especially $Na_{0.5}Gd_{0.5}WO_4$: x% Eu^{3+} have been compared with the doping concentration of Eu^{3+}, suggesting the concentration increase of Eu^{3+} is favorable for the strong intensity, long luminescent lifetime and high luminescence quantum efficiency.

Acknowledgements This work is supported by the Developing Science Fund of Tongji University and the National Natural Science Foundation of China (20971100).

References

1. Holcomb MO, Mueller-Mach R, Mueller GO, Collins D, Fletcher RM, Steigerwald DA (2003) Lasers and Electro-Optics. CLEO '03. Conference 1

2. Mueller-Mach R, Mueller GO (2002) High-power phosphor-converted light-emitting diodes based on III-nitrides IEEE. J Sel Top Quantum Electron 8:339
3. Nakamura S (1997) Blue-green light-emitting diodes and violet laser diodes. MRS Bull 22:29
4. Grillot PN, Krames MR, Zhao H, Teoh SH (2006) Sixty thousand hour light output reliability of AlGaInP light emitting diodes. IEEE Trans 6:564
5. Neeraj S, Kijima N, Cheetham AK (2004) Novel red phosphors for solid-state lighting: the system $NaM(WO_4)_{(2-x)}(MoO_4)_x$: Eu^{3+} (M=Gd, Y, Bi). Chem Phys Lett 387:2
6. Lo CL, Duh JG, Chiou BS, Peng CC (2001) Synthesis of Eu^{3+}-activated yttrium oxysulfide red phosphor by flux fusion method. Mater Chem Phys 71:179
7. Yakovyna V, Zhydachevskii Y, Mikhailik VB, Solskii I, Sugak D, Vakiv M (2008) Effect of thermo-chemical treatments on the luminescence and scintillation properties of $CaWO_4$. Optl Mater 30:1630
8. Yan SX, Zhang JH, Zhang X, Lu SZ (2007) Enhanced red emission in $CaMoO_4$: Bi^{3+}, Eu^{3+}. J Phys Chem C 111:13256
9. Corbel G, Chevereau E, Kodjikian S, Lacorre P (2007) Topological metastability and oxide ionic conduction in $La_{2-x}Eu_xMo_2O_9$. Inorg Chem 46:6395
10. Shang M, Wang WZ, Xu HL (2009) New Bi_2WO_6 nanocages with high visible-light-driven photocatalytic activities prepared in refluxing EG. Cryst Growth Design 9:991
11. Volkov V, Cascales C, Kling A, Zaldo C (2005) Growth, structure, and evaluation of laser properties of $LiYb(MoO_4)_2$ single crystal. Chem Mater 17:291
12. Rico M, Liu J, Cano-Torres JM, Garcia_Cortes A, Cascales C, Zaldo C, Griebner U, Petrov V (2005) Continuous wave and tunable laser operation of Yb^{3+} in disordered $NaLa(MoO_4)_2$. Appl Phys B 81:621
13. Rico M, Griebner U, Petrov V, Ortega P, Han XM, Cascales C, Zaldo C (2006) Growth, spectroscopy, and tunable laser operation of the disordered crystal $LiGd(MoO_4)_2$ doped with ytterbium. J Opt Soc Am B 23:1083
14. Schmidt A, Rivier S, Petrov V, Griebner U, Han XM, Cano-Torres JM, Garcia-Cortes A, Serrano MD, Cascales C, Zaldo C (2008) Continuous-wave tunable and femtosecond modelocked laser operation of Yb: $NaY(MoO_4)_2$. J Opt Soc Am B 25:1341
15. Wang ZL, Liang HB, Gong ML, Su Q (2006) Novel red phosphor of Bi^{3+}, Sm^{3+} co-activated $NaEu(MoO_4)_2$. Opt Mater 29:896
16. Hazenkamp MF, Blasse G (1990) Rare-earth ions adsorbed onto porous glass: luminescence as a characterizing tool. Chem Mater 2:105
17. Kato A, Oishi S, Shishido T (2005) Evaluation of stoichiometric rare-earth molybdate and tungstate compounds as laser materials. J Phys Chem Solids 66:2079
18. Porto SPS, Scott JF (1967) Raman spectra of $CaWO_4$, $SrWO_4$, $CaMoO_4$, and $SrMoO_4$. Phys Rev 157:716
19. Wang ZL, Liang HB, Gong ML, Su Q (2007) Novel red phosphor of Bi^{3+}, Sm^{3+} co-activated $NaEu(MoO_4)_2$. Opt Mater 29:896
20. Zhou LY, Choy WCH, Shi JX, Gong ML, Liang HB, Yuk TI (2005) Synthesis, vacuum ultraviolet and near ultraviolet-excited luminescent properties of $GdCaAl_3O_7$: RE^{3+} (RE=Eu, Tb). J Solid State Chem 178:3004
21. Lei F, Yan B (2009) Morphology controlled synthesis, physical characterization and photoluminescence of novel self-assembled pompon-like white light phosphor: Eu^{3+}-doped sodium gadolinium tungstate. J Phys Chem C 113:1074
22. Wang ZL, Liang HB, Gong ML, Su Q (2007) Luminescence investigation of Eu^{3+} activated double molybdates red phosphors with scheelite structure. J Alloys Compds 432:308
23. Wang JG, Jing XP, Yan CH, Lin JH, Liao FH (2006) Influence of fluoride on f-f transitions of Eu^{3+} in $LiEuM_2O_8$ (M=Mo, W). J Lumin 121:57
24. Malta OL, Brito HF, Menezes JFS, Goncaülves e Silva FR Jr, Alves S Jr, Farias FS, de Andrade AVM (1997) Spectroscopic properties of a new light-converting device Eu(thenoyltrifluoroacetonate)$_3$ 2(dibenzyl sulfoxide). A theoretical analysis based on structural data obtained from a sparkle model. J Lumin 75:255
25. Werts MHV, Jukes RTF, Verhoeven JW (2002) The emission spectrum and the radiative lifetime of Eu^{3+} in luminescent lanthanide complexes. Phys Chem Chem Phys 4:1542
26. Malta OL, Couto dos Santos MA, Thompson LC, Ito NK (1996) Intensity parameters of 4f-4f transitions in the Eu(dipivaloylmethanate)3 1, 10-phenanthroline complex. J Lumin 69:77
27. Teotonio ES, Espínola JGP, Brito HF, Malta OL, Oliveria SF, de Foria DLA, Izumi CMS (2002) Influence of the *N*-[methylpyridyl] acetamide ligands on the photoluminescent properties of Eu(III)-perchlorate complexes. Polyhedron 21:1837
28. Lei F, Yan B (2008) Hydrothermal synthesis and luminescence of $CaMO_4$: RE^{3+} (M=W, Mo; RE=Eu, Tb) submicro-phosphors. J Solid State Chem 181:855
29. Zhang HW, Fu XY, Niu SY (2008) Synthesis and luminescent properties of nanosized YVO_4: Ln (Ln=Sm, Dy). J Alloys Compds 245:61
30. Cavalli E, Belletti A, Mahiou R, Boutinaud P (2010) Luminescence properties of $Ba_2NaNb_5O_{15}$ crystals activated with Sm^{3+}, Eu^{3+}, Tb^{3+} or Dy^{3+} ions. J Lumin 130:733